Research Article | Vol. 9, No. 7 / 1 July 2019 / Optical Materials Express 2738
Optical Materials EXPRESS

Deposition-on-contact regime and the effect of donor-acceptor distance during laser-induced forward transfer of viscoelastic liquids

EMRE TURKOZ,[1] ANTONIO PERAZZO,[1] LUC DEIKE,[1,2] HOWARD A. STONE,[1] AND CRAIG B. ARNOLD[1,3,*]

[1]Department of Mechanical and Aerospace Engineering, Princeton University, Princeton, New Jersey 08544, USA
[2]Princeton Environmental Institute, Princeton University, Princeton, New Jersey 08544, USA
[3]Princeton Institute for the Science and Technology of Materials, Princeton University, Princeton, New Jersey 08544, USA
*cbarnold@princeton.edu

Abstract: Optimizing the direct-writing of viscoelastic liquids requires an understanding of the governing physics during jet and droplet formation. In this article, we study the effect of the distance between the donor and acceptor surfaces and identify a unique deposition-on-contact regime associated with viscoelasticity. For a given laser pulse energy, depending on the liquid film thickness, rheological properties, and the distance between the liquid film and the acceptor surface, the resulting jet can result in either a rapid deposition of a small volume or the formation of a liquid bridge that delays the breakup of the liquid filament and can result in deposition of multiple droplets. By adjusting the gap distance between the donor and acceptor surfaces, we show that it is possible to obtain single drop depositions via deposition-on-contact from viscoelastic liquids. Using dimensionless parameters, we present criteria that can be used to predict the different regimes observed in the experiments.

1. Introduction

Laser-induced forward transfer (LIFT) is a laser direct-write technique [1], where a laser pulse is used to transfer material from a donor surface to an acceptor surface [2,3]. This technique has been previously used in the transfer of many different kinds of materials ranging from solid metals to viscoelastic pastes [4–7]. We used this technique to reveal the governing physics of weakly viscoelastic liquid jets and their breakup by focusing on the balance of underlying elastic, viscous, capillary and inertial forces [8]. LIFT of viscoelastic liquids and gels is especially relevant for bioprinting applications. Many bioinks studied in the literature for laser-assisted bioprinting are made of water-based polymer solutions in the form of hydrogels [9]. These polymer solutions are used as the medium for living cells in laser direct-write and other cell printing applications. Some of the preferred polymers for these applications are alginate [10], gelatin [11] and polyethylene oxide (PEO) [12–14]. Therefore, the physics and breakup of viscoelastic liquids are important for direct-write applications of biomaterials. During the direct-writing of viscoelastic solutions, the position of the acceptor surface can determine the aspect ratio of the formed jet, and additional viscoelastic effects have to be taken into account in addition to viscous and capillary effects [15]. Different regimes of printing using LIFT have been reported previously for weakly viscoelastic alginate solutions [16,17], which exhibit a Newtonian-like deposition and breakup behavior due to their low viscoelasticity.

The governing forces during the thinning of a viscoelastic filament are compared using the relevant time scales. The elasticity of the viscoelastic solutions is characterized by the elongational relaxation time λ, which denotes the time for the strain to relax when the stress is

#364948 https://doi.org/10.1364/OME.9.002738
Journal © 2019 Received 15 Apr 2019; revised 19 May 2019; accepted 20 May 2019; published 3 Jun 2019

Optical Materials EXPRESS

removed [18]. Conventionally, as the relaxation time of a material increases, it is said to become more viscoelastic. The inertia-capillary time scale is defined as $t_c = \sqrt{\rho R_0^3/\gamma} = 0.344/\omega_R$, where ρ is the liquid density, R_0 is the relevant length scale, which is conventionally taken as filament radius, γ is the liquid-air surface tension, and ω_R is the Rayleigh capillary instability growth rate [19]. The visco-capillary time scale is defined as $t_v = \mu R_0/\gamma$, where μ is the liquid viscosity. For LIFT applications, we use the liquid film thickness $H_f \sim R_0$ [8] as the characteristic length scale.

Dimensionless parameters based on the time scales of the governing forces are used in the literature to explain the governing dynamics of viscoelastic filament thinning [20], satellite droplet formation [21,22], and the effect of the properties of the ambient medium [23,24]. Following the pioneering studies on viscoelastic filament thinning in the literature [25–28], we define the dimensionless parameters Deborah number and Ohnesorge number, which are formulated as $De = \lambda/t_c = \lambda/\sqrt{\rho H_f^3/\gamma}$ and $Oh = t_v/t_c = \mu/\sqrt{\rho H_f \gamma}$, respectively. The Deborah number is used to compare the relaxation time scale to the capillary time scale. Larger Deborah numbers indicate that the polymer solution behaves more elastically during the flow. On the other hand, the Ohnesorge number compares the viscous and the capillary time scales. As the Ohnesorge number exceeds 1, the viscous effects slow down the capillary instability [29], and the growth rate deviates from the inertial Rayleigh capillary instability growth rate.

Another important parameter that determines the fate of a liquid filament is its aspect ratio, which can be defined as the ratio of its length to radius, L/H_f. A number of studies have focused on the number of droplets breaking up from a Newtonian filament [21,22,30]. These studies show that the fate of a filament depends on the aspect ratio and the Ohnesorge number Oh as the droplet breakup takes place more readily for larger filament aspect ratios and smaller Ohnesorge numbers. This is expected as lower Ohnesorge numbers indicate stronger capillary effects that can overcome the viscous resistance to thinning. In addition, filaments with smaller aspect ratios have more time to thin before they collapse towards a sphere, and they also have larger surface areas where perturbations can be introduced through external effects.

In the current study, we use a variant of LIFT called blister-actuated LIFT (BA-LIFT), where a laser pulse is focused on a solid polymer film, which is coated with the liquid material to be transferred [31]. This solid film absorbs the laser pulse energy and rapidly forms a locally expanding blister that deforms the liquid film and leads to jet formation. For our experiments, we use highly viscoelastic PEO solutions, which enable us to observe effects like the formation of beads-on-a-string structure [27] and significant stretching without breakup [20]. We identify a unique deposition-on-contact regime and present the high-speed images of the different regimes observed in the experiments with viscoelastic liquids. To analyze the different regimes observed during the experiments, we perform rheology measurements to evaluate the viscosity and relaxation time of the solutions. Using these material properties and other experimental parameters including the blister dimensions and the donor-acceptor surface gap distance, we calculate the relevant dimensionless parameters and build a phase diagram to identify different drop deposition regimes.

2. High-speed images and different regimes

The experimental setup for the BA-LIFT process is similar to those described in previous studies [32]. A frequency-tripled Nd:YVO_4 laser (Coherent AVIA, 20 ns) is used to generate a pulse with 355-nm wavelength. The laser beam diameter is approximately 20 μm. High-speed videos are captured using a Phantom v2012 camera with 500,000 - 700,000 frames per second using a constant LED backlight. For the experiments presented in this section, the same laser pulse energy 7.12 ± 0.131 μJ is used, which creates a blister that has a gaussian profile with the blister height $H_b = 9.7$ μm and blister radius $R_b = 25$ μm. The viscoelastic solutions are made by adding polyethylene oxide (PEO) of 8 MDa molecular weight into deionized water (DI water)

Optical Materials EXPRESS

with 0.15, 0.20 and 0.30 wt.% concentrations. We use a relatively high molecular weight PEO to have solutions with longer relaxation times and increased viscoelasticity [33]. The solutions created using this polymer have previously been assumed to behave like an ideal Boger fluid [27,34], which is a viscoelastic liquid that does not exhibit a shear rate dependent shear viscosity. The liquid films are coated with Mayer rods or doctor blades with different settings to obtain films with different thicknesses. The liquid film thickness is measured using a confocal microscope and exhibits 12-15% variation from one coating to the other.

We characterize both the shear and elongational rheological properties of the PEO solutions. The shear viscosity μ is measured as a function of shear rate $\dot{\gamma}$ for three different PEO concentrations, 0.15 wt.%, 0.20 wt.% and 0.30 wt.% using an Anton Paar Physica MCR-301 stress-controlled rheometer with a double-gap geometry. The viscosity values are measured as 4.0 mPa.s, 6.5 mPa.s, and 7.5 mPa.s for 0.15 wt.%, 0.20 wt.% and 0.30 wt.%, respectively. In addition to the shear viscosity, we measure the elongational relaxation time λ of the polymer solutions using the gravity jet thinning technique [25,35]. The relaxation times are evaluated as 2.5 ± 0.3 ms, 6.6 ± 1.3 ms, and 9.7 ± 1.5 ms for 0.15 wt.%, 0.20 wt.% and 0.30 wt.%, respectively. The rheology measurements are presented in Appendix A (Fig. 6).

For liquid jets generated with the BA-LIFT experimental setup, we identified four different drop formation regimes. These regimes are represented with the schematic shown in Fig. 1. The first regime shown in Fig. 1(a) is the no-transfer regime, where the absorption of the laser pulse energy does not result in a jet that can reach the acceptor surface. This regime takes place when the laser pulse energy is too low to form a jet or when the jet does not reach the acceptor surface and retracts back to the donor film without breaking up. The second regime presented in Fig. 1(b) is the single-drop breakup regime, where the jet breaks up into a drop before it reaches the substrate. A sequence of experimental images is presented in Fig. 2(a), where a single drop breaks up between 5.00 and 6.66 μs after the jet is formed, and lands on the acceptor surface. This regime is one of the preferable ejection mechanisms for printing as one droplet is deposited per laser pulse.

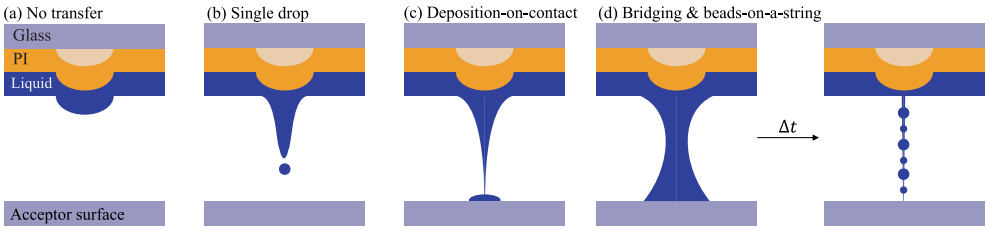

Fig. 1. Different regimes observed during the transfer of viscoelastic PEO solutions after the absorption of the laser pulse energy by the polyimide (PI) layer. (a) No transfer regime where the laser pulse energy is insufficient for the jet to reach the acceptor surface. (b) Single drop regime where breakup takes place before the jet reaches the acceptor surface. (c) The deposition-on-contact regime where the acceptor surface is placed close to the maximum stretching length of the jet. The deposition is rapid, and a single drop is deposited. (d) The liquid bridge regime where the elastic forces along the filament can sustain the formation of a liquid bridge. The resulting viscoelastic filament continues to thin and results in the formation of the beads-on-a-string structure after some time Δt.

Figures 1(c) and 1(d) represent the two regimes where a liquid bridge is formed between the donor and acceptor surfaces. Figure 1(c) represents the deposition-on-contact regime where the formed jet gets deposited on the acceptor surface without forming a longer lasting viscoelastic bridge. The experimental images for this regime are shown in Fig. 2(b), where the entire deposition is completed by about 25 μs. On the other hand, it is also possible to observe the formation of a liquid bridge and quasi-steady beads-on-a-string formation after some time Δt as

Optical Materials EXPRESS

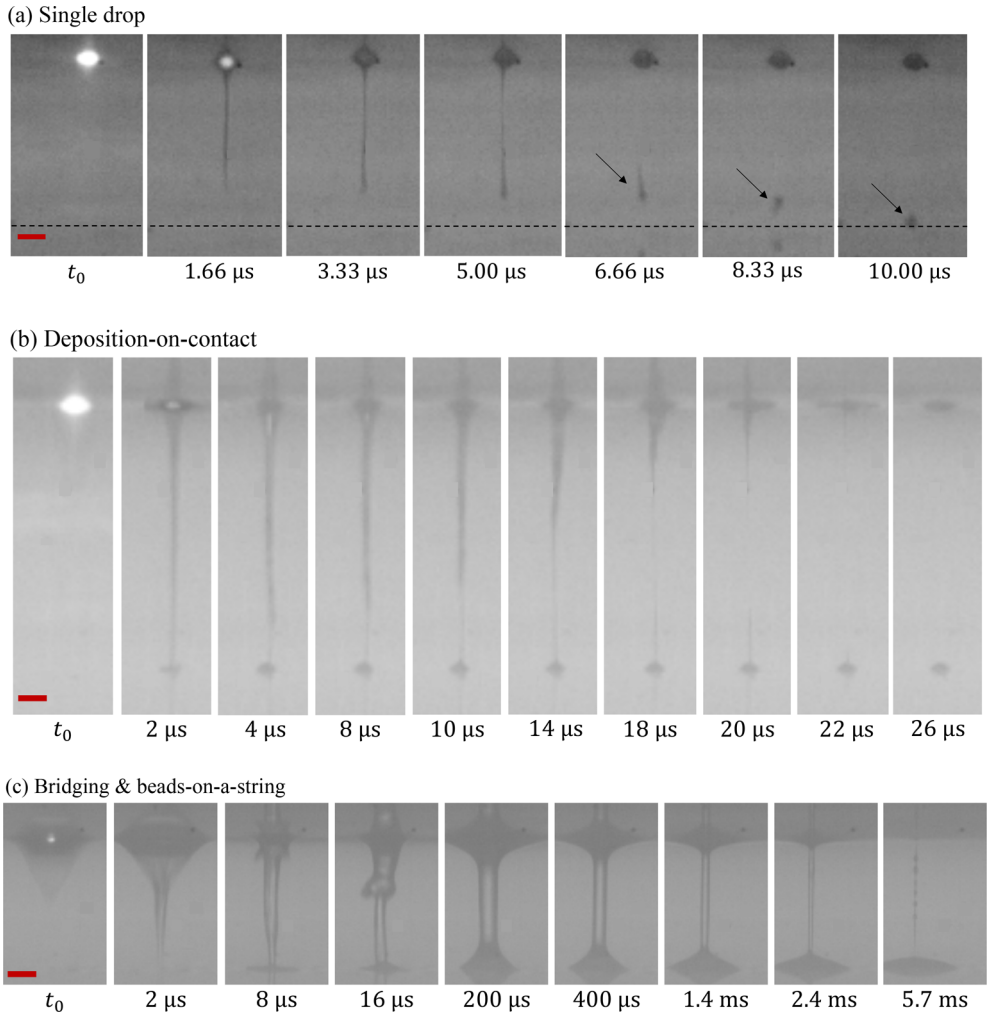

Fig. 2. Images from high-speed videos of different regimes observed during the transfer of viscoelastic PEO solutions. (a) Single drop deposition (Fig. 1(b)) where the filament breaks up into a droplet and is deposited onto the acceptor surface (H_f = 5.8 μm, μ = 6.5 mPa.s, λ = 6.6 ms). The acceptor surface is shown with dashed lines. (b) An example for the deposition-on-contact (Fig. 1(c)) regime, where the jet is stretched almost to the maximum when it reaches the substrate, so deposition takes place rapidly (H_f = 10.2 μm, μ = 7.5 mPa.s, λ = 9.7 ms). The elastic forces pull the viscoelastic filament back to the donor liquid film layer. (c) The bridging regime (Fig. 1(d)), where a thin liquid bridge goes through (viscous and elastic) thinning (H_f = 18.5 μm, μ = 4.0 mPa.s, λ = 2.5 ms). This regime results in the formation of the beads-on-a-string structure towards the end of the filament breakup. The laser pulse energy for all of the cases is measured as 7.12 ± 0.131 μJ. The spot size is 20 μm. The scale bar represents 25 μm.

Optical Materials EXPRESS

represented in Fig. 1(d). As shown in Fig. 2(c), the time scale of this regime is very different compared to the previous regimes. The beads-on-a-string formation lasts up to ~ 6 ms, while the previously mentioned deposition regimes take only up to 30 μs. This beads-on-a-string regime is not desired for printing, as the formed multiple droplets can be deposited onto the acceptor surface.

The deposition-on-contact regime observed in Fig. 2(b) is a unique deposition regime which takes place due to the elasticity of the viscoelastic liquid. Due to the elasticity, the stretched jet develops a retracting force that pulls the main body of the filament back to the donor surface. Liquid jets of Newtonian liquids do not exhibit such behavior. To compare viscoelastic with Newtonian liquids, another set of experiments is performed with a Newtonian solution prepared with DI water and glycerol of 50 wt.% - 50 wt.% concentration. A sequence of images from the ejection of this Newtonian solution is presented in Fig. 3. It is seen from this figure that the jet reaches the acceptor surface around 2 μs after the laser pulse is shot, and the formed liquid bridge starts to collapse around 80 μs. After the liquid bridge breaks up, it further breaks up into multiple droplets and these droplets are deposited onto the acceptor surface. This is very different from the deposition-on-contact regime presented in Fig. 2(b). In the case of the Newtonian filament, the breakup of the filament occurs closer to the donor surface, while the breakup for the viscoelastic filament occurs at the end of the jet. The longer is a Newtonian filament, it is more likely for it to break up into more droplets [21]. The same does not hold for viscoelastic filaments as can be seen from the comparison of Figs. 2b and 3.

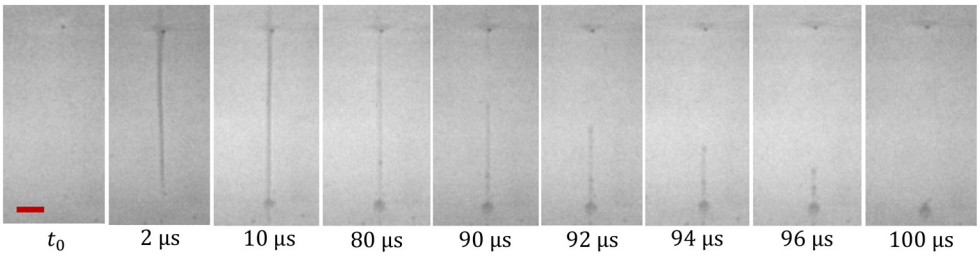

Fig. 3. Deposition of a Newtonian liquid prepared with DI water and glycerol of 50 wt.% - 50 wt.% concentrations ($\mu \approx 5.3$ mPa.s [36], $\rho \approx 1125$ kg/m^3). Due to the lack of elasticity, when stretched, Newtonian liquids do not retract back as observed with the deposition-on-contact regime (Fig. 2(b)) with viscoelastic liquids. Long filaments of Newtonian liquids breakup into multiple droplets and these droplets are deposited onto the acceptor surface. The scale bar represents 25 μm.

The deposition-on-contact regime indicates that there can be two different approaches to optimize the printing of viscoelastic liquids. The first method is the conventional single drop regime as presented in Fig. 2(a), which has been further examined in previous studies [8]. The other method is to adjust the experimental settings, so that the jet reaches the acceptor surface around its maximum stretch and results in the deposition-on-contact regime. The deposition-on-contact regime can be also more advantageous when transferring mechanically sensitive materials such as stem cells [37], since the momentum of the material decreases due to the stretching of the jet. We study the printing regimes presented in this section by first evaluating the material properties and calculating the relevant dimensionless parameters as explained in the next section.

3. Results and discussion

The four regimes presented in Fig. 1 and described in the previous section are observed by changing the experimental parameters for the BA-LIFT setup. These parameters include the liquid film thickness H_f, PEO concentration, which affects the viscosity μ and the relaxation time

Optical Materials EXPRESS

λ of the liquid film, and the gap distance between the acceptor and the donor substrates H_g. The laser pulse energy is held constant, so all of the jets are actuated with the same blister profile.

For the data presented in this study, the liquid film thickness is varied between 4.8 and 38 μm. The highest Ohnesorge number in this study is evaluated with H_f = 4.8 μm for 0.3 wt.% PEO solution as $Oh_{max} \approx 0.39$, which means that for all of the cases presented here $Oh = t_v/t_c < 1$ so that the relevant time scale for breakup is the capillary time scale.

We use dimensionless parameters to characterize the regimes observed in this study. We start formulating these parameters by first noting that the breakup of liquid filaments should take place before the jet reaches the acceptor surface for the single drop regime (Fig. 2(a)). This implies that the capillary time scale t_c should be lower than the time for the jet to reach the acceptor surface t_g, so that $t_g/t_c > 1$ would indicate the single drop deposition regime. The time to reach the acceptor surface can be evaluated as $t_g = H_g/U_j$, where U_j is the characteristic jet velocity, which is not constant during the jetting process [38]. We note that the dimensionless parameter t_g/t_c might not describe the governing physics if the droplet breakup takes place due to inertial effects such as splashing instead of capillary effects, which are observed in our experimental configurations. For the cases presented here, we take U_j as the average blister velocity U_b until the blister height reaches the 90% of its final height. We calculate this average velocity value as U_b = 62.3 m/s using the time-dependent blister profile and velocity formulas presented in our previous study [38] (see Appendix B, Fig. 7). This approach assumes that the liquid film inertia does not affect the jet velocity, which is not accurate for thicker liquid films. However, for the single drop cases obtained in this study, we measured the average jet velocity as $U_j = 57.9 \pm 6.3$ m/s from the high-speed videos. This value is close to the average blister velocity we calculate and shows that using the average blister velocity is a good approximation to evaluate t_g/t_c to identify the single drop deposition cases.

As stated in previous sections, the deposition-on-contact regime takes place when the acceptor is placed close to the location where the jet length reaches its maximum. We evaluate the maximum jet length before the jet starts to retract back, L_{max}, experimentally by first running the BA-LIFT experiments without an acceptor surface. With these experiments, it is possible to evaluate the ratio H_g/L_{max} for each case. For the single drop cases where the breakup takes place before the jet reaches the acceptor surface, L_{max} is evaluated as the longest intact length of the jet, so $H_g/L_{max} > 1$. On the other hand, for the cases where a full liquid bridge forms, this relation becomes $H_g/L_{max} < 1$.

Bringing these two dimensionless parameters together, Fig. 4 presents the phase diagram where the ratio H_g/L_{max} is plotted against t_g/t_c for different experiments. It is seen from this figure that above the $t_g/t_c > 1$ limit, the deposition takes place with the single drop regime. In addition, we see that the deposition-on-contact cases fulfill the condition $H_g/L_{max} \sim 1$. The affect of this ratio is illustrated with the schematic presented in Fig. 5(a). In this figure, the ratio H_g/L_{max} is decreasing from left to right, and the regime changes from no breakup, to deposition-on-contact and then to the bridging regime.

Predicting L_{max} correctly for a given set of experimental conditions would be critical in order to guide the placement of the acceptor surface, and our numerical efforts to calculate L_{max} are to be published in the future. From our experiments, we observe that L_{max} is strongly dependent on laser pulse energy, and decreases with increasing H_f and μ. On the other hand, to analytically understand the effect of stretching, we can consider the filament aspect ratio, which can be formulated as H_g/H_f. When the liquid jet reaches the substrate, the jet length would be equal to H_g, and the jet radius scales with the liquid film thickness as shown before [8]. Therefore, this parameter should play a key role in determining the outcome of the bridging regime. For a given laser pulse energy, there should be a threshold aspect ratio value that marks the start of the deposition-on-contact regime. This threshold aspect ratio should change as a function of the elasticity of the viscoelastic solutions. For the laser pulse energy used in this study, the

Optical Materials EXPRESS

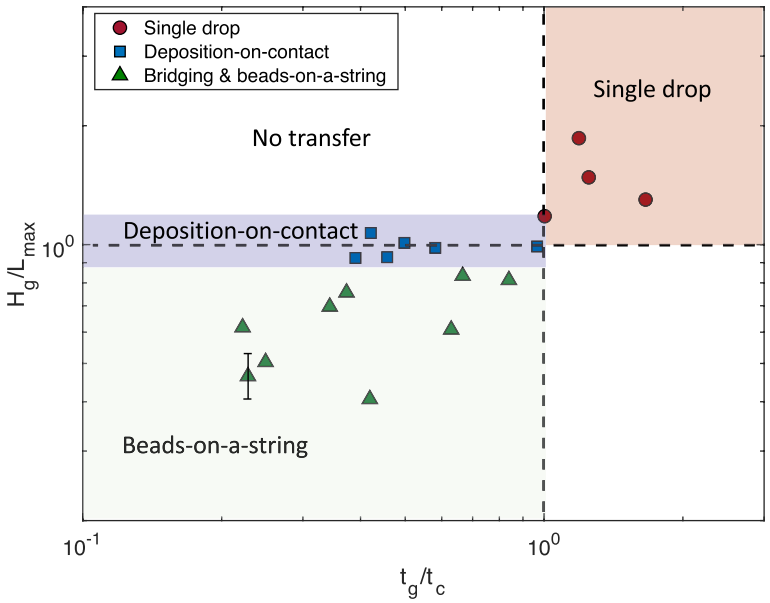

Fig. 4. Phase diagram of the regimes observed during the jetting of PEO solutions using BA-LIFT. For single drop deposition, the time for the breakup to take place, t_c, should be smaller than the time that the jet takes to reach the acceptor surface, $t_g = H_g/U_j$, where U_j is the characteristic jet velocity. Here, U_j is approximated as the average blister velocity U_b until the blister height reaches the 90% of its final height (see Appendix B). Single drop deposition is therefore observed if t_g/t_c>1. The deposition-on-contact regime takes place when the donor-acceptor surface distance H_g is approximately equal to the jet length at maximum stretch L_{max}, $H_g/L_{max} \sim 1$. L_{max} is measured experimentally without an acceptor surface and found to exhibit for a given configuration approximately 15 % variation, whose effect is represented with the errorbar on a data point.

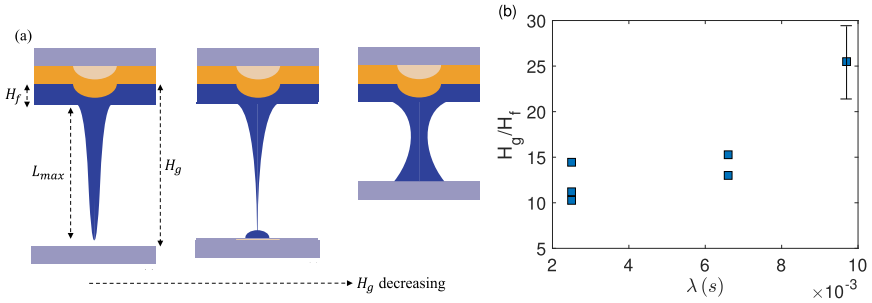

Fig. 5. Aspect ratio plays a critical role in determining the outcome of the drop deposition process. (a) Different regimes observed by changing the donor-acceptor gap distance and keeping all of the other experimental parameters constant. If H_g is too large, the jet can retract back without transferring any material. As H_g is decreased, the deposition-on-contact regime is observed. Further decrease in H_g results in the formation of a liquid bridge. (b) The aspect ratio H_g/H_f values that result in deposition-on-contact regime as a function of the relaxation time λ. As the relaxation time of the solution is increased, the resulting jet needs to be stretched more for the deposition-on-contact regime. The liquid film thickness H_f measurements show approximately 15% variation, whose effect is represented with the errorbar on a data point.

Optical Materials EXPRESS

aspect ratio values that result in the deposition-on-contact regime are presented as a function of relaxation time in Fig. 5(b). As the viscoelasticity of the solutions is increased, the threshold aspect ratio increases, as more elastic filaments can sustain the formation of the beads-on-a-string structure with larger aspect ratios. We also note that the wettability of the surface to the printed solution should also play a role to support the liquid bridge formation. The dependence of the aspect ratio on the relaxation time and other experimental parameters should be investigated further for a prediction that can be performed *a priori*.

In this article, we present the unique deposition-on-contact regime for viscoelastic liquids, and reveal the effect of the distance between the donor and acceptor surfaces on different regimes for the BA-LIFT printing of viscoelastic liquid polymer solutions. These regimes can be organized in a phase diagram using two sets of dimensionless parameters, H_g/L_{max} and t_g/t_c. We demonstrate that $t_g/t_c>1$ is an accurate condition to predict jetting instances with breakup, and the deposition-on-contact regime takes place when $H_g/L_{max} \sim 1$. We further show that there are certain values of the aspect ratio H_g/H_f that allows for the deposition-on-contact regime and these values are a function of the relaxation time of printed viscoelastic solutions. While the images and the phase diagram in this section are presented for the BA-LIFT process, we believe that other LIFT techniques can also benefit from the same principles while dealing with viscoelastic liquids [16,39]. The corresponding t_g values for evaporation-based LIFT setups can be evaluated by measuring or theoretically estimating the cavity expansion profile. We believe this approach can lead to the proper placement of the acceptor surface and it can increase the throughput of the LIFT technique as a whole.

A. Rheology measurements

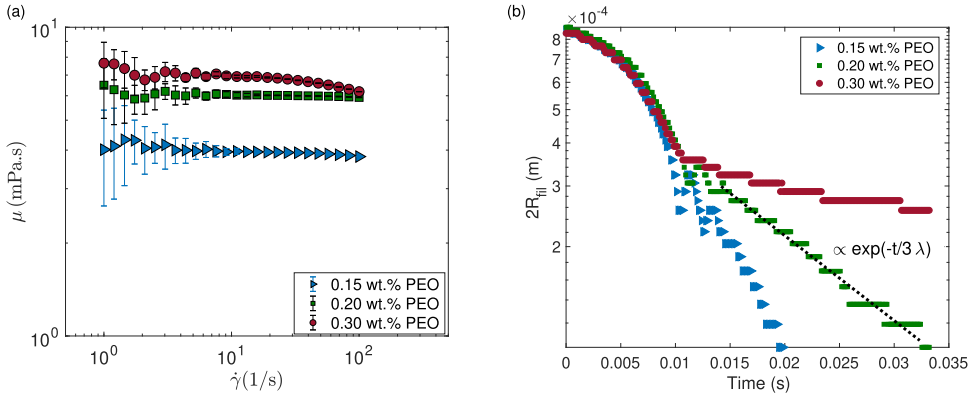

Fig. 6. Rheological properties of PEO solutions. (a) Shear viscosity μ of 0.15 wt.%, 0.20 wt.% and 0.30 wt.% PEO in water as a function of shear rate $\dot{\gamma}$. The constant viscosity values to calculate the Ohnesorge number for the PEO solutions are 4.0 mPa.s, 6.5 mPa.s, and 7.5 mPa.s for 0.15 wt.%, 0.20 wt.% and 0.30 wt.% PEO, respectively. (b) Elongational relaxation time measurements of 0.15 wt.%, 0.20 wt.% and 0.30 wt.% PEO in water. The diameter $2R_{\text{fil}}$ of a gravity-driven jet is recorded as a function of time t. The relaxation time λ is calculated by fitting an exponential line to the elastic thinning part. The relaxation times are evaluated as 2.5 ± 0.3 ms, 6.6 ± 1.3 ms, and 9.7 ± 1.5 ms for 0.15 wt.%, 0.20 wt.% and 0.30 wt.%, respectively.

B. Blister profile and mean blister velocity

Optical Materials EXPRESS

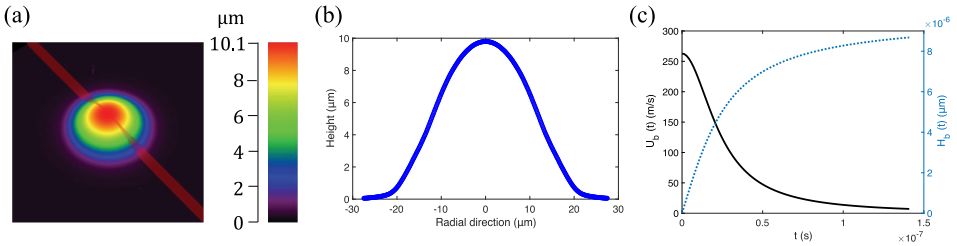

Fig. 7. The blister profile generated with the laser pulse energy used in this study. (a) A three-dimensional contour plot of a blister measured with confocal microscopy. The red line across the blister is used to extract the profile presented in (b). (c) The evolution of the blister velocity $U_b(t)$ (solid curve) and blister height H_b (t) (dotted curve) as a function of time for the first ~ 150 ns, when the blister height reaches 90% of its final height. The average velocity U_b used in evaluating the dimensionless parameters is calculated as the average velocity during this time. The time-dependent profile is obtained from the empirical formula presented in a previous study [38].

Funding

Princeton University Schmidt Fund.

References

1. C. B. Arnold, P. Serra, and A. Piqué, "Laser direct-write techniques for printing of complex materials," MRS Bull. **32**(1), 23–31 (2007).
2. P. Serra and A. Piqué, *Introduction to Laser-Induced Transfer and Other Associated Processes* (Wiley-VCH Verlag GmbH & Co. KGaA Weinheim, Germany, 2018).
3. P. Serra and A. Piqué, "Laser-induced forward transfer: Fundamentals and applications," Adv. Mater. Technol. **4**(1), 1800099 (2019).
4. Q. Li, A. P. Alloncle, D. Grojo, and P. Delaporte, "Generating liquid nanojets from copper by dual laser irradiation for ultra-high resolution printing," Opt. Express **25**(20), 24164–24172 (2017).
5. M. Chatzipetrou, M. Massaouti, G. Tsekenis, A. K. Trilling, E. van Andel, L. Scheres, M. M. Smulders, H. Zuilhof, and I. Zergioti, "Direct creation of biopatterns via a combination of laser-based techniques and click chemistry," Langmuir **33**(4), 848–853 (2017).
6. J. Luo, R. Pohl, L. Qi, G.-W. Römer, C. Sun, D. Lohse, and C. W. Visser, "Printing functional 3d microdevices by laser-induced forward transfer," Small **13**(9), 1602553 (2017).
7. A. Piqué and P. Serra, *Laser Printing of Functional Materials: 3D Microfabrication, Electronics and Biomedicine* (John Wiley & Sons, 2018).
8. E. Turkoz, A. Perazzo, H. Kim, H. A. Stone, and C. B. Arnold, "Impulsively induced jets from viscoelastic films for high-resolution printing," Phys. Rev. Lett. **120**(7), 074501 (2018).
9. Z. Zhang, Y. Jin, J. Yin, C. Xu, R. Xiong, K. Christensen, B. R. Ringeisen, D. B. Chrisey, and Y. Huang, "Evaluation of bioink printability for bioprinting applications," Appl. Phys. Rev. **5**(4), 041304 (2018).
10. Z. Zhang, W. Chai, R. Xiong, L. Zhou, and Y. Huang, "Printing-induced cell injury evaluation during laser printing of 3t3 mouse fibroblasts," Biofabrication **9**(2), 025038 (2017).
11. N. R. Schiele, D. B. Chrisey, and D. T. Corr, "Gelatin-based laser direct-write technique for the precise spatial patterning of cells," Tissue Eng., Part C **17**(3), 289–298 (2011).
12. S. Hong, D. Sycks, H. F. Chan, S. Lin, G. P. Lopez, F. Guilak, K. W. Leong, and X. Zhao, "3d printing: 3d printing of highly stretchable and tough hydrogels into complex, cellularized structures (adv. mater. 27/2015)," Adv. Mater. **27**(27), 4034 (2015).
13. J. Z. Gul, M. Sajid, M. M. Rehman, G. U. Siddiqui, I. Shah, K.-H. Kim, J.-W. Lee, and K. H. Choi, "3d printing for soft robotics–a review," Sci. Technol. Adv. Mater. **19**(1), 243–262 (2018).
14. I. T. Ozbolat and M. Hospodiuk, "Current advances and future perspectives in extrusion-based bioprinting," Biomaterials **76**, 321–343 (2016).
15. C. Florian, S. Piazza, A. Diaspro, P. Serra, and M. Duocastella, "Direct laser printing of tailored polymeric microlenses," ACS Appl. Mater. Interfaces **8**(27), 17028–17032 (2016).
16. Z. Zhang, R. Xiong, D. T. Corr, and Y. Huang, "Study of impingement types and printing quality during laser printing of viscoelastic alginate solutions," Langmuir **32**(12), 3004–3014 (2016).
17. C. Unger, M. Gruene, L. Koch, J. Koch, and B. N. Chichkov, "Time-resolved imaging of hydrogel printing via laser-induced forward transfer," Appl. Phys. A **103**(2), 271–277 (2011).

Optical Materials EXPRESS

18. M. Rubinstein and R. H. Colby, *Polymer Physics*, vol. 23 (Oxford University Press New York, 2003).
19. L. Rayleigh, "Xvi. on the instability of a cylinder of viscous liquid under capillary force," The London, Edinburgh, Dublin Philos. Mag. J. Sci. **34**(207), 145–154 (1892).
20. P. P. Bhat, S. Appathurai, M. T. Harris, M. Pasquali, G. H. McKinley, and O. A. Basaran, "Formation of beads-on-a-string structures during break-up of viscoelastic filaments," Nat. Phys. **6**(8), 625–631 (2010).
21. A. A. Castrejón-Pita, J. Castrejon-Pita, and I. Hutchings, "Breakup of liquid filaments," Phys. Rev. Lett. **108**(7), 074506 (2012).
22. T. Driessen, R. Jeurissen, H. Wijshoff, F. Toschi, and D. Lohse, "Stability of viscous long liquid filaments," Phys. Fluids **25**(6), 062109 (2013).
23. H. A. Stone, "Dynamics of drop deformation and breakup in viscous fluids," Annu. Rev. Fluid Mech. **26**(1), 65–102 (1994).
24. H. A. Stone and M. P. Brenner, "Note on the capillary thread instability for fluids of equal viscosities," J. Fluid Mech. **318**(1), 373–374 (1996).
25. V. Entov and E. Hinch, "Effect of a spectrum of relaxation times on the capillary thinning of a filament of elastic liquid," J. Non-Newtonian Fluid Mech. **72**(1), 31–53 (1997).
26. S. L. Anna and G. H. McKinley, "Elasto-capillary thinning and breakup of model elastic liquids," J. Rheol. **45**(1), 115–138 (2001).
27. C. Clasen, J. Eggers, M. A. Fontelos, J. Li, and G. H. McKinley, "The beads-on-string structure of viscoelastic threads," J. Fluid Mech. **556**, 283–308 (2006).
28. A. M. Ardekani, V. Sharma, and G. H. McKinley, "Dynamics of bead formation, filament thinning and breakup in weakly viscoelastic jets," J. Fluid Mech. **665**, 46–56 (2010).
29. J. Eggers and E. Villermaux, "Physics of liquid jets," Rep. Prog. Phys. **71**(3), 036601 (2008).
30. F. Wang, F. Contò, N. Naz, J. Castrejón-Pita, A. Castrejón-Pita, C. Bailey, W. Wang, J. Feng, and Y. Sui, "A fate-alternating transitional regime in contracting liquid filaments," J. Fluid Mech. **860**, 640–653 (2019).
31. E. Turkoz, R. Fardel, and C. B. Arnold, "Advances in blister-actuated laser-induced forward transfer (ba-lift)," *Laser Print. Funct. Materials: 3D Microfabr. Electron. Biomed.* pp. 91–121 (2018).
32. E. Turkoz, L. Deike, and C. B. Arnold, "Comparison of jets from newtonian and non-newtonian fluids induced by blister-actuated laser-induced forward transfer (ba-lift)," Appl. Phys. A **123**(10), 652 (2017).
33. V. Tirtaatmadja, G. H. McKinley, and J. J. Cooper-White, "Drop formation and breakup of low viscosity elastic fluids: Effects of molecular weight and concentration," Phys. Fluids **18**(4), 043101 (2006).
34. B. Keshavarz, E. C. Houze, J. R. Moore, M. R. Koerner, and G. H. McKinley, "Ligament mediated fragmentation of viscoelastic liquids," Phys. Rev. Lett. **117**(15), 154502 (2016).
35. M. Roché, H. Kellay, and H. A. Stone, "Heterogeneity and the role of normal stresses during the extensional thinning of non-brownian shear-thickening fluids," Phys. Rev. Lett. **107**(13), 134503 (2011).
36. J. B. Segur and H. E. Oberstar, "Viscosity of glycerol and its aqueous solutions," Ind. Eng. Chem. **43**(9), 2117–2120 (1951).
37. N. T. Kattamis, P. E. Purnick, R. Weiss, and C. B. Arnold, "Thick film laser induced forward transfer for deposition of thermally and mechanically sensitive materials," Appl. Phys. Lett. **91**(17), 171120 (2007).
38. M. S. Brown, C. F. Brasz, Y. Ventikos, and C. B. Arnold, "Impulsively actuated jets from thin liquid films for high-resolution printing applications," J. Fluid Mech. **709**, 341–370 (2012).
39. Z. Zhang, R. Xiong, R. Mei, Y. Huang, and D. B. Chrisey, "Time-resolved imaging study of jetting dynamics during laser printing of viscoelastic alginate solutions," Langmuir **31**(23), 6447–6456 (2015).